IVYSPRING INTERNATIONAL PUBLISHER

Theranostics

2018; 8(11): 2992-3006. doi: 10.7150/thno.20982

Research Paper

Cancer radiotheranostics targeting carbonic anhydrase-IX with ^{111}In- and ^{90}Y-labeled ureidosulfonamide scaffold for SPECT imaging and radionuclide-based therapy

Shimpei Iikuni, Masahiro Ono✉, Hiroyuki Watanabe, Yoichi Shimizu, Kohei Sano, Hideo Saji

Department of Patho-Functional Bioanalysis, Graduate School of Pharmaceutical Sciences, Kyoto University, 46-29 Yoshida Shimoadachi-cho, Sakyo-ku, Kyoto 606-8501, Japan.

✉ Corresponding author: Phone: +81-75-753-4608, Fax: +81-75-753-4568, e-mail: ono@pharm.kyoto-u.ac.jp

Received: 2017.05.11; Accepted: 2018.02.27; Published: 2018.04.30

Abstract

Hypoxic cells dynamically translocate during tumor growth and after radiotherapy. The most desirable direction for therapy targeting hypoxic cells is combining imaging and therapy (theranostics), which may help realize personalized medicine. Here, we conducted cancer radiotheranostics targeting carbonic anhydrase-IX (CA-IX), which is overexpressed in many kinds of hypoxic cancer cells, using low-molecular-weight ^{111}In and ^{90}Y complexes with a bivalent ureidosulfonamide scaffold as the CA-IX-binding moiety ([^{111}In/^{90}Y]US2).

Methods: The targeting ability of [^{111}In]US2 was evaluated by *in vivo* biodistribution study in CA-IX high-expressing (HT-29) tumor-bearing mice. *In vivo* imaging of HT-29 tumors was carried out using single photon emission computed tomography (SPECT). [^{90}Y]US2 was administered to HT-29 tumor-bearing mice to evaluate cancer therapeutic effects.

Results: [^{111}In]US2 highly and selectively accumulated within HT-29 tumors (4.57% injected dose/g tumor at 1 h postinjection), was rapidly cleared from the blood pool and muscle after 4 h based on a biodistribution study, and visualized HT-29 tumor xenografts in mice at 4 h postinjection with SPECT. Radionuclide-based therapy with [^{90}Y]US2 significantly delayed HT-29 tumor growth compared with that of untreated mice (P = 0.02 on day 28, Student's t-test), without any critical hematological toxicity due to its rapid pharmacokinetics.

Conclusion: These results indicate that cancer radiotheranostics with [^{111}In/^{90}Y]US2 provides a novel strategy of theranostics for cancer hypoxia.

Key words: radiotheranostics, carbonic anhydrase-IX, radiometallic ureidosulfonamide scaffold, hypoxia.

Introduction

A key feature of many solid tumors is hypoxia, which is caused by an imbalance between oxygen supply and consumption [1-5]. Hypoxia arises due to limitations of oxygen diffusion in tumors. The microvasculature of tumors is abnormal and often fails to maintain the oxygen pressure [6-8]. Hypoxic tumors are closely associated with tumor propagation, malignant progression, and resistance to chemotherapy and radiotherapy. In addition, hypoxia is also associated with a poor outcome regardless of the treatment approach, indicating that it might be one of the important cancer therapeutic targets [1-5, 8-12].

Dynamic changes in the extent and distribution of hypoxia have been reported with high spatial resolution [13]. In addition, radiotherapy might cause

the translocation of the surviving cells towards blood vessels after achieving survival, leading to tumor recurrence [14]. Therefore, tumor microenvironments are considered to change dynamically during tumor growth and after radiation therapy [14]. Also, a decrease in hypoxic cells caused by radiation-induced reoxygenation has been observed [15]. On the basis of these findings, simultaneous radiation intervention with imaging of hypoxic cells is strongly desired for cancer therapy targeting hypoxia, which can help achieve personalized medicine. In the last few decades, many theranostic agents targeting cancer have been reported [16]; however, most of these were based on nanoparticles with pharmacokinetic limitations, including slow clearance from the blood pool and non-target tissues, and non-specific organ uptake, leading to high toxicity to several types of normal tissues [16, 17]. In contrast, the development of a theranostic approach using radiolabeled low-molecular-weight agents with positron emission tomography (PET) and single photon emission computed tomography (SPECT) has attracted much attention. For instance, the use of radiolabeled prostate-specific membrane antigen inhibitors and somatostatin analogs in radiotheranostics led to excellent results in patients [18-21]; therefore, a radiotheranostic concept using low-molecular-weight agents is favorable.

Targeting a biomolecule of the hypoxia-induced signaling cascade has been advocated as a useful strategy for oncologic treatment [8, 11]. Hypoxia regulates the expression of several proteins, including one of the carbonic anhydrase (CA) isozymes, CA-IX, through the hypoxia-inducible factor-1 (HIF-1) cascade [1-5, 12, 22-24]. CA-IX catalyzes the reversible hydration of carbon dioxide to a bicarbonate ion and a proton [1-5, 12]. CA-IX is related to tumor cell growth and survival by regulating the intra- and extra-cellular pH with various proteins, such as aquaporins and anion exchangers [1-5, 12, 23, 25, 26]. The expression of CA-IX is controlled by HIF-1α and is markedly upregulated by hypoxia [1-4, 10, 27]. HIF-1α is hydroxylated and ultimately degraded through binding to the wild-type von Hippel Lindau (VHL) tumor suppressor protein and subsequent ubiquitination, reducing the expression of CA-IX [1-4, 10, 23, 27]. CA-IX expression is markedly increased in many types of tumors, such as carcinomas of the bladder [28], uterine cervix [29, 30], head and neck [31], breast [32], lung [33], and kidney [34] tumors. In addition, CA-IX is pathologically expressed in cancer cells and is located at the cell surface. CA-IX is thus considered to be an attractive target for both cancer therapy and diagnosis. The radiolabeled antibody G250 targeting CA-IX has shown potential for PET/SPECT or radionuclide-based therapy [35-37]; however, its slow clearance from the blood pool leads to a low signal-to-noise ratio on imaging and a high toxicity due to the radiation burden. Many efforts to develop low-molecular-weight agents for therapeutics or diagnostics on CA-IX have been made [38-47]. Recently, an acetazolamide derivative, XYIMSR, was radiolabeled for imaging (^{111}In/^{64}Cu) and therapy (^{177}Lu). [^{177}Lu]XYIMSR-01 showed promising results regarding its therapeutic effect [48-50].

Radiolabeled pharmaceuticals have been utilized for various disease diagnoses and therapies. They must undergo selective accumulation at the targeted site. A radiotheranostic agent, specifically interacting with a targeted biomolecule, is labeled with γ- or β^+-emission radioisotopes for nuclear imaging (SPECT or PET, respectively) and with β^-- or α-emission radioisotopes for radionuclide-based therapy. One platform labeled with various radioisotopes for each application is easily prepared using a radiometallic chelate. Indium-111 (γ-emitter) and yttrium-90 (β^--emitter) have similar chelating properties, and are suitable for SPECT imaging and internal radiotherapy, respectively [51, 52]. The concurrent employment of ^{111}In and ^{90}Y complexes synthesized from the same radiolabeling precursor is one of the strategies for radiotheranostics. In addition, 1,4,7,10-tetraazacyclododecane-1,4,7,10-tetraacetic acid (DOTA) has been used as a metal chelator, which forms a stable complex with ^{111}In, ^{90}Y, and other radiometals.

In the present study, we synthesized an ^{111}In/^{90}Y-labeled compound with the aim of creating a novel cancer theranostic agent targeting CA-IX. Using this radiotheranostic agent, we demonstrated clear and selective *in vivo* imaging of a CA-IX-expressing tumor with SPECT, and the delay of CA-IX-expressing tumor growth without any critical hematological toxicity in model mice. This success in cancer diagnosis and therapy with the ^{111}In/^{90}Y complex suggests a novel strategy for cancer radiotheranostics for hypoxia, leading to personalized medicine.

Methods

Chemistry and radiolabeling

The details of the syntheses of ^{111}In/^{90}Y complexes and the corresponding $^{113/115}$In complexes based on ureidosulfonamide are available in Supplementary Material.

Cell culture

HT-29 and MDA-MB-231, which are human

colorectal cancer cell lines and human breast cancer cell lines, respectively, were purchased from Sumitomo Dainippon Pharma (Osaka, Japan). RCC4 plus VHL (RCC4-VHL) and RCC4 plus vector alone (RCC4-VA), which are human renal cell carcinoma cell lines (RCC4) stably transfected with pcDNA3-VHL (VHL-expressing vector) and pcDNA3 (empty vector), respectively, were purchased from DS Pharma Biomedical (Osaka, Japan). Cells were maintained in Dulbecco's modified Eagle's medium (DMEM) (Thermo Fisher Scientific, Massachusetts, U.S.A.) supplemented with 10% heat-inactivated fetal bovine serum (Thermo Fisher Scientific), 100 U/mL penicillin, and 100 μg/mL streptomycin in a 5% CO_2/air incubator at 37 °C.

Animals

All animal experiments were performed in accordance with our institutional guidelines and were approved by the Kyoto University Animal Care Committee. Male BALB/c-*nu*/*nu* nude mice and male ddY mice were purchased from Shimizu Laboratory Supplies (Shizuoka, Japan).

Under anesthesia with isoflurane (2% in an air mixture), BALB/c-*nu*/*nu* nude mice were subcutaneously inoculated with MDA-MB-231 cells (1×10^7 cells/mouse), in 150 μL of DMEM and Geltrex (Thermo Fisher Scientific) at a 1:1 ratio, in the left flank. Fifteen days later, HT-29 cells (1×10^7 cells/mouse) were also subcutaneously injected into the right flank of MDA-MB-231 tumor-bearing mice. Tumor-bearing mice were used for studies when tumors reached a diameter of approximately 10–15 mm. For the radionuclide-based therapy study, BALB/c-*nu*/*nu* nude mice were subcutaneously inoculated with only HT-29 cells (5×10^6 cells/mouse) in the right flank. All efforts were made to minimize suffering.

Western blotting assay

Cultured cells (HT-29, MDA-MB-231, RCC4-VHL, and RCC4-VA) were incubated at 37 °C in an atmosphere containing 5% CO_2 and 21% O_2 (normoxic conditions) or 1% O_2 (hypoxic conditions) for 24 h. After cell washing with phosphate-buffered saline (PBS) (pH 7.4) (Thermo Fisher Scientific) three times and scraping with a cell scraper, the cell pellet was obtained by centrifuging the lysate (400 ×g, 3 min). To prepare tumor samples, the HT-29 and MDA-MB-231 tumors were removed from the tumor-bearing mice, and they were dissociated with a rod on ice. One tablet of protease inhibitor cocktail tablet (Roche Diagnostics, Basel-Stadt, Swiss Confederation) was dissolved in a mixture of (5×) cell culture lysis reagent (Promega, Wisconsin, U.S.A.) (1 mL) and H_2O (4 mL), and 0.5 mL of this solution was added to the cell (HT-29, MDA-MB-231, RCC4-VHL, and RCC4-VA) pellet and tumor (HT-29 and MDA-MB-231) lysate. After centrifuging (12,000 ×g, 10 min), the protein concentration of the supernatant was determined using BCA Protein Assay Kit (Thermo Fisher Scientific). Equal amounts of protein (10 μg) were loaded onto a polyacrylamide gel (e-PAGEL HR; Atto, Tokyo, Japan), separated by electrophoresis, and transferred to a polyvinylidene fluoride membrane (Immobilon-P Membrane; Merck, Hessen, Germany). After three 5-min incubations in 0.05% PBS-Tween 20 (PBST), the membranes were blocked with 5% skim milk powder (Nacalai Tesque, Kyoto, Japan) in PBST for 1 h at room temperature. Incubation overnight with a primary rabbit IgG monoclonal anti-human CA-IX antibody (ab108351, 1:5,000 dilution; Abcam, Cambridgeshire, U.K.) was performed at 4 °C. As a control, a primary rabbit IgG monoclonal anti-glyceraldehyde 3-phosphate dehydrogenase (GAPDH) antibody (14C10, 1:1,000 dilution; Cell Signaling Technology, Massachusetts, U.S.A.) was used. Subsequently, the membranes were incubated in PBST for 5 min three times, and then incubated with secondary anti-rabbit IgG horseradish peroxidase conjugated antibody (W401B, 1:5,000 dilution; Promega) at room temperature for 1 h. After three 5-min incubations in PBST, antibody binding was determined using a chemoluminescence detection system (ChemiDoc Touch Imaging System; Bio-Rad, California, U.S.A.). The results were analyzed using ImageJ [53].

In vitro cell binding assay

HT-29, MDA-MB-231, RCC4-VHL, and RCC4-VA cells were incubated in 12-well plates (2×10^5 cells/well) at 37 °C in an atmosphere containing 5% CO_2 for 24 h. After incubation, cells were then incubated at 37 °C in an atmosphere containing 5% CO_2 and 21% O_2 (normoxic conditions) or 1% O_2 (hypoxic conditions) for another 24 h. After removing the medium, [^{111}In]US1 or [^{111}In]US2 (20 kBq, 80.2–130.7 GBq/μmol for [^{111}In]US1 and 104.0–112.8 GBq/μmol for [^{111}In]US2) in the medium (1 mL) was added to each well inside the hypoxic chamber (miniMACS Anaerobic Workstation; Don Whitley Scientific, West Yorkshire, U.K.), and the plates were incubated under normoxic or hypoxic conditions for 2 h. Nonspecific binding was evaluated by the addition of acetazolamide (50 μM). After incubation, each well was washed with 1 mL of PBS (pH 7.4) (Thermo Fisher Scientific), and the cells were lysed with 1 M NaOH (0.5 mL × 2). Radioactivity bound to cells was measured using a γ counter (Wallac 1470 Wizard; PerkinElmer, Massachusetts, U.S.A.). The protein

concentration was determined using BCA Protein Assay Kit (Thermo Fisher Scientific).

Biodistribution study in model mice

A saline solution (100 μL) of [^{111}In]US1 or [^{111}In]US2 (40 kBq, 206.3 GBq/μmol for [^{111}In]US1 and 59.5 GBq/μmol for [^{111}In]US2) was directly injected into the tail vein of HT-29 and MDA-MB-231 tumor-bearing mice (n = 5 each time). For *in vivo* competition studies, tumor-bearing mice were injected with [^{111}In]US1 or [^{111}In]US2 (40 kBq, 206.3 GBq/μmol for [^{111}In]US1 and 59.5 GBq/μmol for [^{111}In]US2) and acetazolamide (10 mg/kg) in saline (100 μL) concurrently. The mice were sacrificed at 1, 4, 8, and 24 h postinjection. The blood, spleen, pancreas, stomach, intestines, kidneys, liver, heart, lungs, brain, HT-29 tumor, MDA-MB-231 tumor, and muscle were collected. Each organ was weighed and the radioactivity was measured using a γ counter (PerkinElmer). The % injected dose/g of samples was calculated by comparing the sample counts with the count of the initial dose.

Analysis of stability in mouse plasma

The blood (5 mL) was collected from 10 ddY mice and centrifuged (1,200 ×g, 10 min) in venous blood collection tubes (Becton, Dickinson and Company, New Jersey, U.S.A.). The plasma (200 μL) was separated and [^{111}In]US2 (185 kBq, 194.5–390.4 GBq/μmol) was added to it. The solution was incubated at 37 °C for 1, 4, 8, and 24 h. After the addition of MeCN (200 μL), it was centrifuged (10,000 ×g, 5 min). The supernatant was filtered with a Cosmonice Filter (S) (0.45 μm, 4 mm) (Nacalai Tesque), and the filtrate was analyzed by reversed-phase high-performance liquid chromatography (RP-HPLC). In addition, the radioactivity of the filter was measured using a γ counter (PerkinElmer).

Analysis of radiometabolites in model mice

A saline solution (100 μL) of [^{111}In]US2 (4.5 MBq, 570.9–1383.9 GBq/μmol) was directly injected into the tail vein of HT-29 tumor-bearing mice (n = 5 for the blood and tumor). For the analysis of radiometabolites in the blood, after the mice were sacrificed at 1 h postinjection, the blood was collected and centrifuged (1,200 ×g, 10 min) in venous blood collection tubes (Becton, Dickinson and Company) to separate the plasma. MeCN (200 μL) was added to a tube containing the plasma (200 μL) and centrifuged (4,000 ×g, 5 min). The supernatant was filtered with a Cosmonice Filter (S) (0.45 μm, 4 mm) (Nacalai Tesque), and the filtrate was analyzed by RP-HPLC. For the analysis of radiometabolites in the HT-29 tumor, after sacrifice at 1 and 24 h postinjection, the HT-29 tumor was removed from the mouse and homogenized in test tubes containing tris-buffered saline (500 μL) using a homogenizer (POLYTRON PT 10-35; KINEMATICA, Lucerne, Swiss Confederation). MeCN (500 μL) was added to a tube containing the homogenized tumor and centrifuged (4,000 ×g, 5 min). Then, MeCN (500 μL) was added to the supernatant and it was centrifuged (4,000 ×g, 5 min). The supernatant was filtered with a Cosmonice Filter (S) (0.45 μm, 4 mm) (Nacalai Tesque), and the filtrate was analyzed by RP-HPLC.

Biodistribution study in normal mice

The details of the biodistribution study in normal mice with [^{111}In]US2 are available in Supplementary Material.

SPECT/CT

A saline solution (150 μL) of [^{111}In]US2 (30 MBq, 538.5–893.6 GBq/μmol) was directly injected into the tail vein of HT-29 and MDA-MB-231 tumor-bearing mice (n = 3). For *in vivo* competition studies, tumor-bearing mice were injected with [^{111}In]US2 (30 MBq, 538.5–893.6 GBq/μmol) and acetazolamide (10 mg/kg) in saline (150 μL) concurrently (n = 3). The HT-29 and MDA-MB-231 tumors in the same mouse were of equal volume (218.0 ± 58.9 mm^3, calculated using the formula: V = [length × (width)^2]/2). The mice were anesthetized by isoflurane (2% in an air mixture) and were placed on a heating pad (36 °C) to maintain the body temperature throughout the procedure. SPECT and CT images were collected using the U-SPECT-II system (MILabs, Utrecht, the Netherlands) with 1.0-mm pinhole collimators (SPECT conditions: 60 min × 1 frame; CT conditions: accurate full angle mode in 60 kV/615 μA) at 1, 4, 8, and 24 h postinjection. SPECT images were reconstructed using the OSEM method (8 subset, 1 iteration) with a 0.8-mm Gaussian filter.

Ex vivo autoradiography with model mice

A saline solution (150 μL) of [^{111}In]US2 (15 MBq, 205.6–262.8 GBq/μmol) was directly injected into the tail vein of HT-29 and MDA-MB-231 tumor-bearing mice (n = 3). Subsequently, a saline solution (100 μL) of pimonidazole hydrochloride (100 mg/kg) (Hypoxyprobe, Massachusetts, U.S.A.) was directly injected into the tail vein of the mice at 3 h postinjection of [^{111}In]US2. The mice were sacrificed at 4 h postinjection of [^{111}In]US2. The HT-29 and MDA-MB-231 tumors were immediately removed, embedded in Super Cryoembedding Medium compound (SECTION-LAB, Hiroshima, Japan), and then frozen in a dry ice/hexane bath. Sections of 10

μm were cut and exposed to a BAS imaging plate (Fuji Film, Tokyo, Japan) for 10 h. Autoradiographic images were obtained using a BAS5000 scanner system (Fuji Film). After autographic examination, the same sections were stained with hematoxylin and eosin (H & E).

The adjacent sections were immunostained by anti-CA-IX antibody, anti-pimonidazole antibody, or anti-CD31 antibody. For immunohistochemical staining of CA-IX and CD31, the sections were incubated with 4% paraformaldehyde (Wako Pure Chemical Industries, Osaka, Japan) for 20 min. After two 5-min incubations in PBS, they were incubated in 3% hydrogen peroxide (Nacalai Tesque, diluted with methanol) for 15 min. The sections were incubated in PBS for 5 min twice, and then incubated with anti-CA-IX primary antibody (ab108351; Abcam, dilution 1:100 with PBS) or anti-CD31 primary antibody (ab28364; Abcam, dilution 1:12.5 with PBS) at room temperature for 90 min. After two 5-min incubations in PBS, the sections were incubated at room temperature for 60 min with a solution of a horseradish peroxidase-labeled polymer conjugated with anti-rabbit secondary antibody (Dako, California, U.S.A.). Subsequently, the sections were incubated in PBS for 5 min twice, and then incubated with diaminobenzidine (Merck) as a chromogen for 5 min. After washing with water, the sections were observed under a microscope (FSX100; Olympus, Tokyo, Japan). For immunohistochemical staining of pimonidazole, Histofine Mousestain Kit (Nichirei Biosciences, Tokyo, Japan) was used according to the manufacturer's specifications. The primary antibody incubation was performed with anti-pimonidazole primary antibody (Hypoxyprobe, dilution 1:12.5 with PBS) at room temperature for 60 min. Diaminobenzidine (Merck) was used as a chromogen. The sections were observed under a microscope (Olympus).

Radionuclide-based therapy

A saline solution (100 μL) of [^{90}Y]US2 (7.4, 3.7, or 1.85 MBq, 495.0–859.5 GBq/μmol) or saline (100 μL) as a control was directly injected into the tail vein of the HT-29 tumor-bearing mice (n = 6 for each dose). The tumor volume and body weight were measured three times a week until 4 weeks after the injection of [^{90}Y]US2. The tumor volume was calculated as described in SPECT/CT, and compared with the initial value (on day 0) to calculate the relative tumor volume. The initial tumor volumes (on day 0) for the 0, 1.85, 3.7, and 7.4 MBq [^{90}Y]US2 groups were 68.9 ± 7.1, 63.2 ± 4.3, 60.7 ± 12.0, and 52.5 ± 4.2 mm^3 (mean ± standard error), respectively. The myelotoxicity of radionuclide-based therapy was assessed using the peripheral blood cell counts. The blood was obtained from the tail vein of each mouse. A blood sample (2 μL) was diluted with Turk's solution (0.01% gentian violet and 1% acetic acid) at a 1:50 ratio and 1% ammonium oxalate at a 1:1,250 ratio for white blood cell and platelet counts, respectively. Cells were counted using a light microscope (EVOS XL Core Cell Imaging System; Thermo Fisher Scientific) and a cell counter (Cell Counter model R1; Olympus). Cell counts were performed three times a week until 4 weeks after the injection of [^{90}Y]US2, and compared with the initial value (on day −4) to calculate relative blood cell counts.

Statistical analysis

Student's *t*-test was used to assess the significance of differences. Differences at the 95% confidence level ($P < 0.05$) were considered significant.

Results

Chemistry and radiolabeling

The synthesis of precursors for ^{111}In/^{90}Y labeling and the corresponding $^{113/115}$In complexes based on ureidosulfonamide is outlined in **Scheme S1-2**. At first, *N*1,*N*7-di-protection of cyclen was performed using *N*-(*tert*-butoxy-carbonyloxy)succinimide [54]. As shown in **Scheme S1**, DOTA-bis(*tert*-butyl)ester **5** was obtained with a favorable yield (73%) from cyclen according to a previous report [54]. The intermediate 4-isocyanatobenzenesulfonamide for the ureido-sulfonamide backbone was prepared by treating 4-aminobenzenesulfonamide with 1,1'-carbonyl-diimidazole, and then the product was directly used for the coupling reaction with 1,4-phenylenediamine to form **6** at a 23% yield [55]. After the amide coupling of **5** with ureidosulfonamide **6** in the presence of 1-hydroxybenzotriazole (HOBT) hydrate, 1-ethyl-3-(dimethylaminopropyl)carbodiimide (EDC) hydro-chloride, and triethylamine in dimethylformamide, hydrolysis of the product with trifluoroacetic acid (TFA) gave **7** and **8** at 21 and 17% yields, respectively. The $^{113/115}$In complexes **9** and **10** were prepared by reacting the corresponding precursor with $^{113/115}InCl_3$ in 2-(*N*-morpholino)ethanesulfonic acid (MES) buffer (0.1 M, pH 5.5) (**Scheme S2**). Heating was necessary to complete the reaction. The ^{1}H NMR, ^{13}C NMR, and MS were consistent with the assigned structures.

^{111}In-labeling was carried out by incubating the corresponding precursor with $^{111}InCl_3$ in 0.1 M MES buffer (pH 5.5) at 90 °C (**Figure 1** and **Scheme S3**). After purification by RP-HPLC, [^{111}In]US1 and [^{111}In]US2 were obtained with high radiochemical purity (> 95%) as determined by RP-HPLC

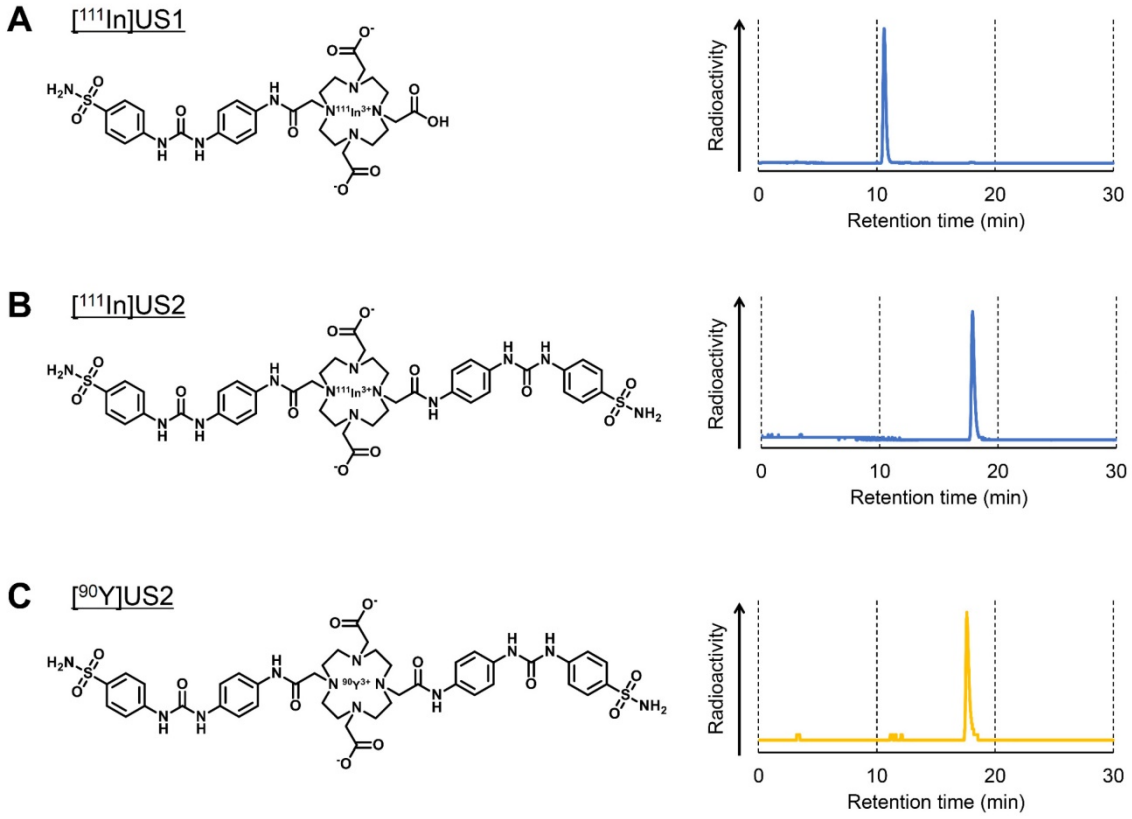

Figure 1. Radiolabeling of [^{111}In]US1, [^{111}In]US2, and [^{90}Y]US2. (A) Chemical structure and typical HPLC profile of [^{111}In]US1. **(B)** Chemical structure and typical HPLC profile of [^{111}In]US2. **(C)** Chemical structure and typical HPLC profile of [^{90}Y]US2. The analyses were performed on a Cosmosil C_{18} column (5C_{18}-PAQ, 4.6 × 250 mm) with a solvent of H_2O/MeCN/TFA [90:10:0.1 (0 min) to 60:40:0.1 (30 min)] as the mobile phase at a flow rate of 1 mL/min.

(**Figure 1A-B**). [^{111}In]US1 was synthesized at a high radiochemical yield (89.2%). Moreover, the radiolabeling reaction of [^{111}In]US2 was performed using various solvents at room temperature, 60 °C, or 90 °C. As shown in **Table S1**, [^{111}In]US2 was obtained at an extremely low or a zero yield in all solvents at room temperature. The ^{111}In-labeling reaction in 0.1 M NaOAc buffer or 0.1 M MES buffer at 60 °C gave [^{111}In]US2 at low yields (12.0% and 23.2%, respectively), while the radiochemical yields using the buffer of the lower concentration (0.01 M) were very low. In addition, the ^{111}In-labeling reaction at 90 °C generated [^{111}In]US2 in moderate yields (47.7–66.0%), except for when using 0.01 M MES buffer as the solvent (7.0%). Among them, [^{111}In]US2 was obtained with the highest radiochemical yield (66.0%) in 0.1 M MES buffer at 90 °C. According to this result, [^{90}Y]US2 was prepared under this condition at a 48.8% radiochemical yield. After purification by RP-HPLC, [^{90}Y]US2 was obtained with a high radiochemical purity (> 95%) as determined by RP-HPLC (**Figure 1C**). The radiochemical identity of the ^{111}In/^{90}Y complex was verified by comparative RP-HPLC using the corresponding $^{113/115}$In complex as a reference (**Table S2**). The retention times between ^{111}In/^{90}Y-labeled tracers and the corresponding $^{113/115}$In complexes suggest that the desired ^{111}In/^{90}Y-labeled ureidosulfonamide derivatives were successfully synthesized.

In vitro cell uptake

The CA-IX expression in HT-29, MDA-MB-231, RCC4-VHL, and RCC4-VA cell lines under normoxic and hypoxic conditions was confirmed by a Western blotting assay before an *in vitro* cell binding assay. Iwanov et al. reported that HT-29 expresses the CA-IX gene, whereas MDA-MB-231 is negative, as demonstrated in Northern blotting analyses [56]. A high level of CA-IX expression was observed in the HT-29 cell line under normoxic conditions, and this expression level was enhanced by incubating under hypoxic conditions. The fold increase over normoxic conditions in HT-29 cells was 1.9 under hypoxic conditions. However, almost no CA-IX expression was observed in the MDA-MB-231 cell line under normoxic conditions, and a slight increase in the CA-IX expression under hypoxic conditions as compared with normoxic conditions was observed (**Figure 2A**). It is generally accepted that a deficit in the VHL gene contributes to HIF-1 stabilization, leading to a high level of CA-IX expression [1-5, 23].

RCC4-VHL and RCC4-VA cell lines showed almost no and a high level of CA-IX expression, respectively, under both normoxic and hypoxic conditions (**Figure S1A**). An *in vitro* cell binding assay was carried out with these cell lines under normoxic and hypoxic conditions (**Figure 2** and **Figure S1**). As shown in **Figure 2B** and **Figure S1B**, [^{111}In]US1 showed no marked uptake into any of the cell lines under normoxic or hypoxic conditions (< 3% initial dose/mg protein). The low-level correspondence of the *in vitro* binding of [^{111}In]US1 to cells with CA-IX expression might be due to the low affinity of [^{111}In]US1 for CA-IX. However, a significant increase in uptake into HT-29 cells under hypoxic conditions as compared with normoxic conditions was observed (2.91 and 0.775% initial dose/mg protein, respectively), which was consistent with the results of Western blotting assays. On the other hand, [^{111}In]US2 displayed a higher uptake into all cell lines than [^{111}In]US1 (**Figure 2C** and **Figure S1C**). Bivalency may maximize the uptake of ^{111}In-labeled ureidosulfonamide derivatives [57, 58]. The uptake of [^{111}In]US2 under normoxic conditions into CA-IX high-expressing cells (HT-29 and RCC4-VA) (25.4 and 69.0% initial dose/mg protein, respectively) was significantly higher than that into CA-IX low-expressing cells (MDA-MB-231 and RCC4-VHL) (11.6 and 14.4% initial dose/mg protein, respectively), suggesting the high selectivity of [^{111}In]US2 for CA-IX. This selectivity was also observed under hypoxic conditions (125, 16.9, 24.0, and 74.3% initial dose/mg protein for HT-29, MDA-MB-231, RCC4-VHL, and RCC4-VA cells, respectively). The uptake of [^{111}In]US2 into HT-29 cells was enhanced in response to hypoxia, as observed for [^{111}In]US1. Moreover, the significant decrease in uptake into CA-IX high-expressing cells by the addition of acetazolamide, a classical CA inhibitor, under both normoxic and hypoxic conditions indicates the marked specificity of [^{111}In]US2 for CA. However, blocking studies suggested a high nonspecific uptake of ^{111}In complexes (5–20% initial dose/mg protein for [^{111}In]US2). These findings indicate that [^{111}In]US2 has superior *in vitro* properties compared with those of [^{111}In]US1.

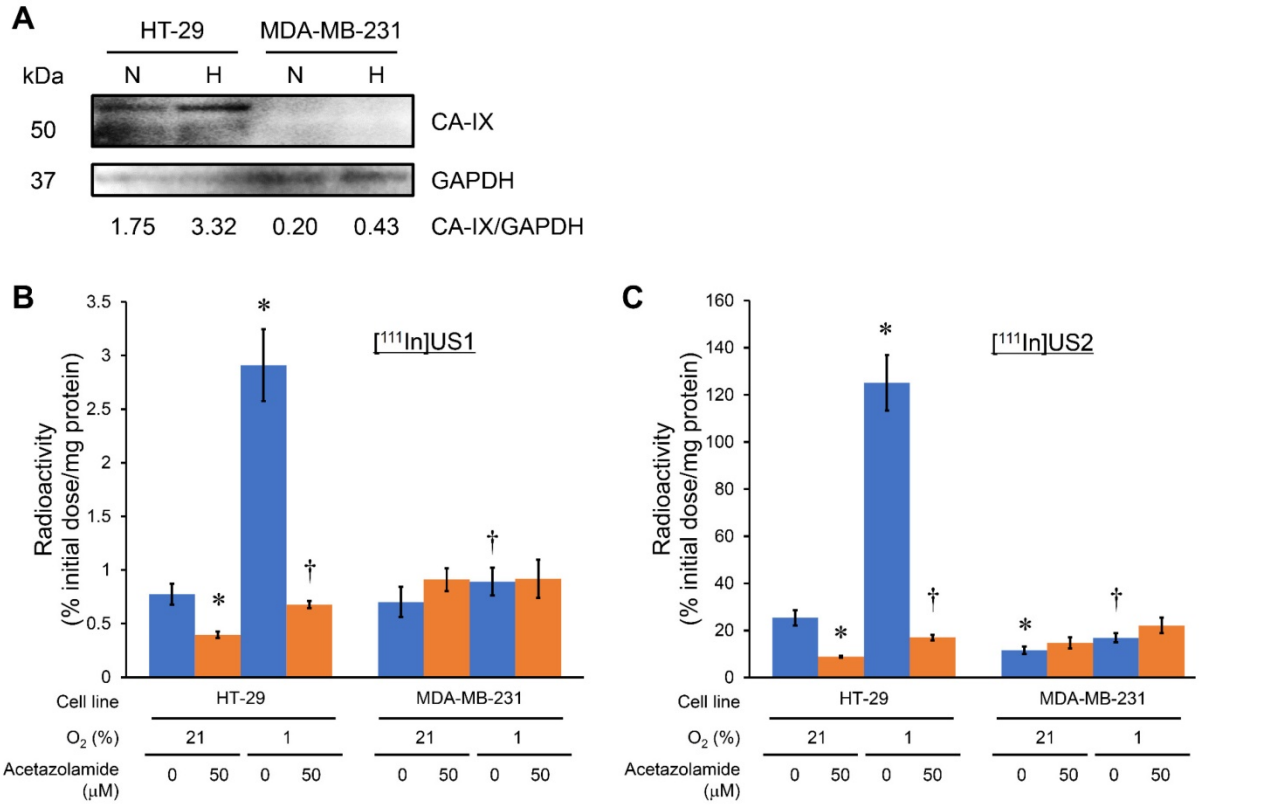

Figure 2. Cell binding assay with [^{111}In]US1 and [^{111}In]US2. (A) Western blotting analysis of HT-29 and MDA-MB-231 cells under normoxic (N) and hypoxic (H) conditions. GAPDH was used as a loading control. **(B)** In vitro uptake of [^{111}In]US1 into cells. **(C)** In vitro uptake of [^{111}In]US2 into cells. Values are expressed as the mean ± standard error of six independent experiments. *P < 0.05 as compared with uptake into HT-29 cells under normoxic conditions, †P < 0.005 as compared with uptake into HT-29 cells under hypoxic conditions (Student's t-test).

In vivo tumor uptake

A biodistribution study was performed to evaluate the *in vivo* uptake into the CA-IX-expressing tumor in the model mice (**Figure 3**, **Table S3** and **Table S4**). HT-29 and MDA-MB-231 have been used as CA-IX-positive and negative cell lines, respectively, both *in vitro* and *in vivo* [59]. A high level of CA-IX expression was observed in the HT-29 tumor lysate from model mice, while weak CA-IX expression was observed in the MDA-MB-231 tumor lysate in our study (**Figure 3A**); therefore, HT-29 and MDA-MB-231 tumors were used as CA-IX-positive and negative ones, respectively, *in vivo*. Although almost no CA-IX expression was observed in the MDA-MB-231 cell line *in vitro* (**Figure 2A**), the *in vivo* MDA-MB-231 tumor showed weak CA-IX expression probably due to the hypoxic condition to some extent in living mice. The bivalent ureidosulfonamide ^{111}In complex ([^{111}In]US2) showed significantly higher accumulation in HT-29 tumors (4.57 %injected dose/g at 1 h postinjection) than that in MDA-MB-231 tumors (1.64 %injected dose/g at 1 h postinjection), indicating a high specificity for CA-IX-expressing tumors *in vivo*. A higher uptake in the HT-29 tumor than that in the MDA-MB-231 tumor was observed at all times. The radioactivity accumulation within the MDA-MB-231 tumor slightly increased from 1 to 8 h postinjection; however, there was no significant difference (P = 0.06, Student's t-test). The blocking studies were carried out at the latest time (24 h postinjection) to exclude the possibility of nonspecific uptake. Specificity was also demonstrated by the fact that radioactivity in the HT-29 tumor at 24 h postinjection (1.72% injected dose/g) significantly decreased on the coinjection of acetazolamide (0.63% injected dose/g) (**Figure 3D**). Blocking studies also indicated a decrease in radioactivity within MDA-MB-231 tumors showing weak CA-IX expression. Moreover, the HT-29 tumor/blood and HT-29 tumor/muscle ratios increased with time and reached 10.78 and 7.75 at 24 h postinjection, respectively, suggesting that [^{111}In]US2 has favorable pharmacokinetics for the *in vivo* imaging of solid tumors (**Figure 3E**). Results consistent with those of the *in vitro* cell binding assay were obtained; in other words, the monovalent ^{111}In complex ([^{111}In]US1) showed a lower uptake and selectivity for the HT-29 tumor (0.27–2.12% injected dose/g at 1–24 h postinjection) (**Figure 3B**).

Based on the results of *in vitro* and *in vivo* uptake examinations, further evaluation was conducted with [^{111}In]US2 and [^{90}Y]US2.

In vitro and *in vivo* stability

To confirm the validity of *in vitro* experiments, the *in vitro* stability of [^{111}In]US2 was evaluated by incubating it in mouse plasma at 37 °C for various pre-determined times (**Figure 4**). The filter contained almost no radioactivity, indicating that [^{111}In]US2 hardly bound to the plasma proteins. Almost all [^{111}In]US2 existed as an intact form (> 96.4%) until 24 h *in vitro* (**Figure 4A**). Moreover, we analyzed the radiometabolites in the blood and HT-29 tumors after the injection of [^{111}In]US2 into the HT-29 tumor-bearing mice. As shown in **Figure 4B-C**, most [^{111}In]US2 existed as an intact form in both the blood and HT-29 tumors at 1 h postinjection (81.4% and 84.4%, respectively). The *in vivo* stability was largely influenced by *in vivo* metabolism unlike the *in vitro* stability, leading to the difference between them (> 99.9% vs. 81.4% at 1 h, respectively). In addition, HT-29 tumors removed at 24 h postinjection included 70.4% [^{111}In]US2, suggesting that it recognizes CA-IX and remains bound to CA-IX with high *in vivo* stability (**Figure 4C**). Radioactive peaks other than the intact [^{111}In]US2 might indicate free ^{111}In according to their retention times on RP-HPLC.

Biodistribution in normal mice

[^{111}In]US2 was administered to normal mice (**Table S5**). [^{111}In]US2 displayed rapid clearance from the blood and muscle with time (0.10 and 0.22% injected dose/g at 24 h postinjection, respectively), suggesting its low background signal and hematological toxicity during *in vivo* imaging and radionuclide-based therapy, respectively, of solid tumors. Moderate and persistent activity in the kidney (7.11–11.39% injected dose/g at 1–24 h postinjection) and moderate accumulation in the stomach (8.05% injected dose at 1 h postinjection) might raise the issue of nephrotoxicity and others. Higher accumulation and retention in the kidney as compared with those in the liver at all times indicated the predominance of renal excretion, which may be derived from its high hydrophilicity (log P_{ow} = −2.81), as shown in **Table S2**. Significant differences in normal organs and tissues between normal and model mice were observed, possibly due to the characters of model mice, including deficits of the thymus and T-cell function and having two more tissues (HT-29 and MDA-MB-231 tumors).

In vivo imaging with SPECT/CT

SPECT/CT images of tumor-bearing mice at 1, 4, 8, and 24 h postinjection with [^{111}In]US2 are shown in **Figure 5**. The CT-only and SPECT-only images are shown in **Figure S2**. The maximum intensity projections of the whole body are also shown in **Figure S3**. Radioactivity outside the mouse in the maximum intensity projection was derived from the feces during the acquisition of SPECT images (**Figure**

S3A). The HT-29 tumor injected into the right flank was not visualized by [^{111}In]US2 at 1 h postinjection (**Figure 5B**), which may derive from its low HT-29 tumor/blood ratio for imaging at that time (**Figure 3E**). Meanwhile, the HT-29 tumor was clearly visualized with a high background ratio at 4, 8, and 24 h postinjection, with almost no signal from the MDA-MB-231 tumor (**Figure 5B**), indicating the very high *in vivo* selectivity of [^{111}In]US2 for CA-IX, consistent with the result of the biodistribution study (**Figure 3D**). Simultaneous injection of an excess of acetazolamide with [^{111}In]US2 decreased the signal level of radioactivity within the HT-29 tumor (**Figure 5C**), also indicating high selectivity against the CA-IX low-expressing tumor. Fast clearance of [^{111}In]US2 from the blood and muscle may contribute to the successful early imaging of tumors.

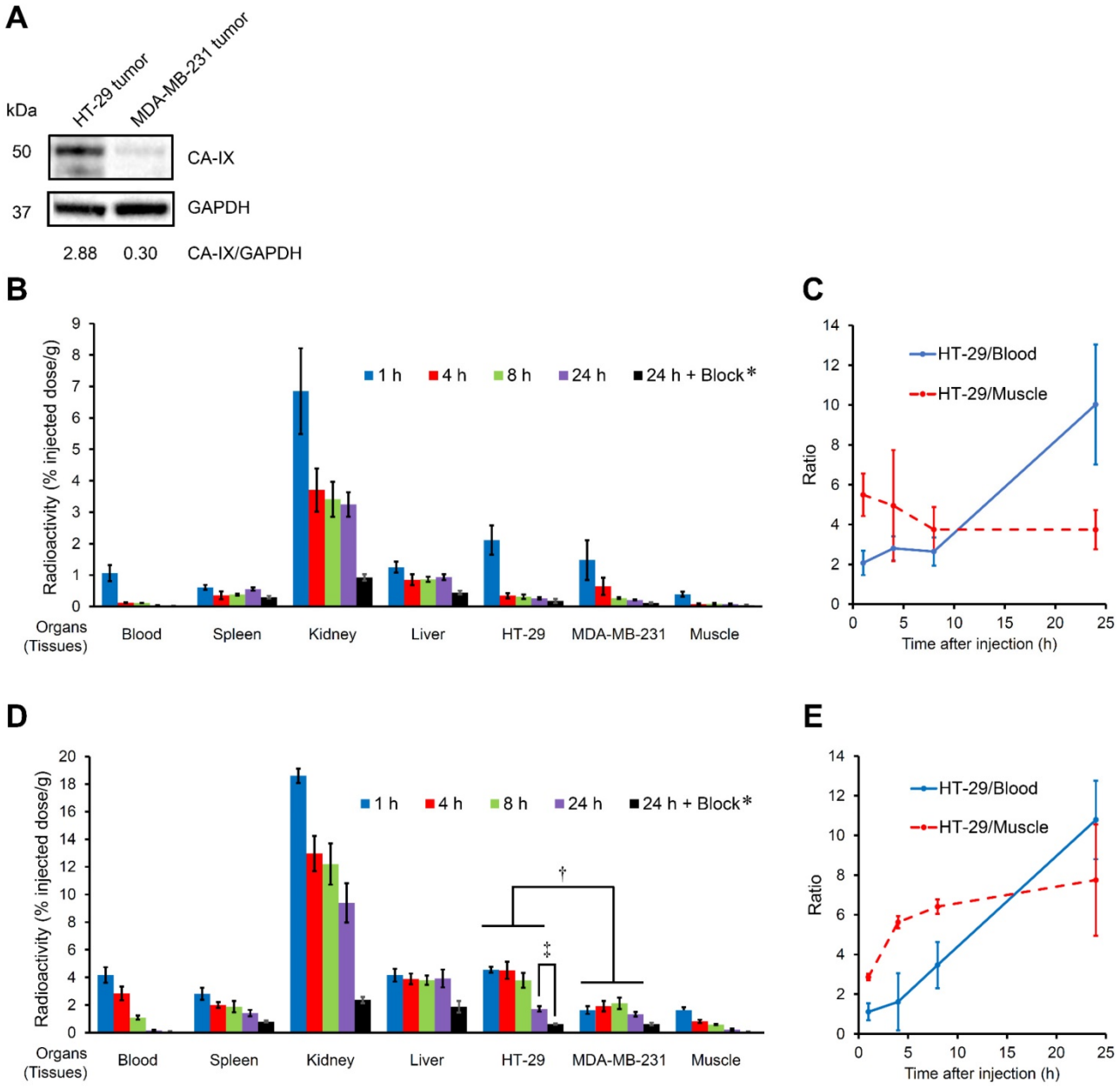

Figure 3. In vivo biodistribution study with [^{111}In]US1 and [^{111}In]US2 in HT-29 and MDA-MB-231 tumor-bearing mice. (A) Western blotting analysis of HT-29 and MDA-MB-231 tumor lysate in vivo. GAPDH was used as a loading control. **(B)** Radioactivity of representative extracted organs and tissues after the intravenous injection of [^{111}In]US1 in the HT-29 and MDA-MB-231 tumor-bearing mice (n = 5). **(C)** Ratios of radioactivity in the HT-29 tumor to that in the blood and muscle in (B). **(D)** Radioactivity of representative extracted organs after the intravenous injection of [^{111}In]US2 in the HT-29 and MDA-MB-231 tumor-bearing mice (n = 5). **(E)** Ratios of radioactivity in the HT-29 tumor to that in the blood and muscle in (D). Values are expressed as the mean ± standard deviation of five mice. *Coinjection of acetazolamide (10 mg/kg). †$P < 0.05$ each time, ‡$P < 0.001$ (Student's *t*-test).

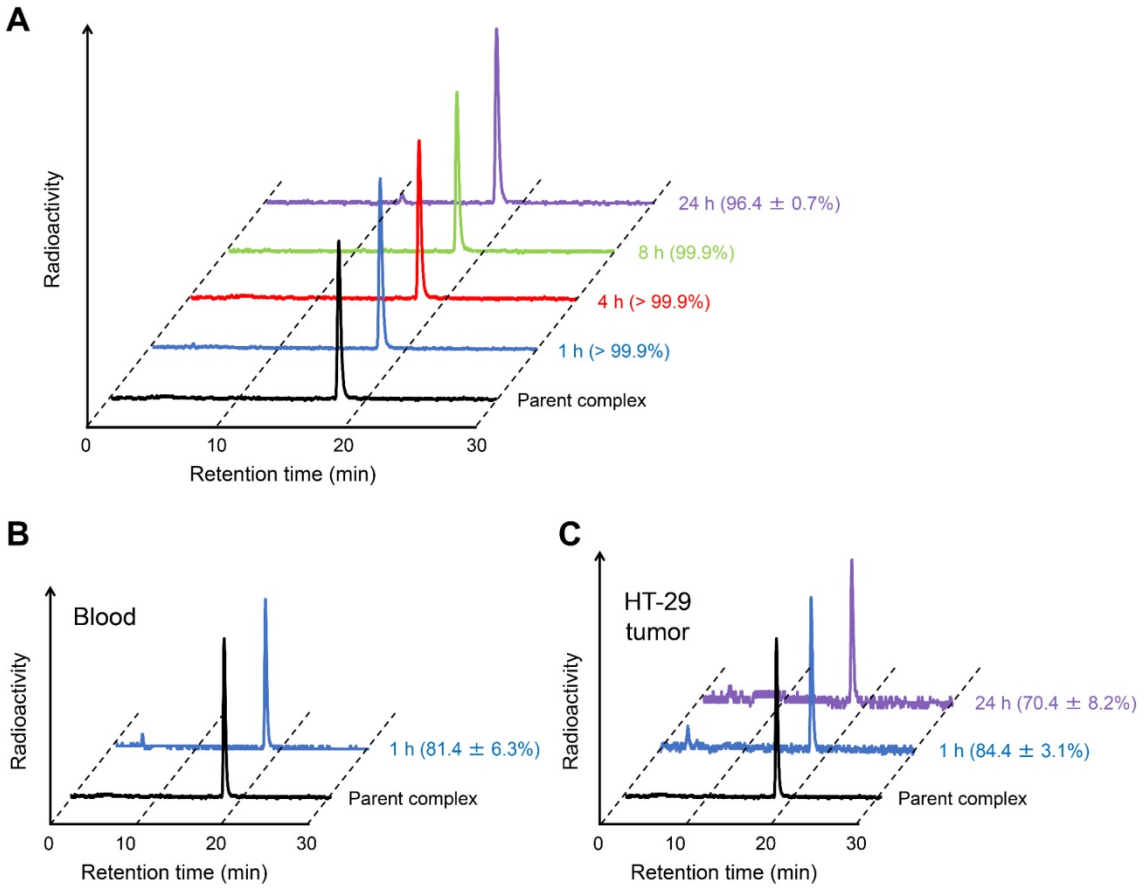

Figure 4. Stability of [^{111}In]US2. (A) Typical HPLC profile of radioactivity and radiochemical purity of [^{111}In]US2 after incubation in mouse plasma at 37 °C for 1, 4, 8, and 24 h. **(B)** Typical HPLC profile of radioactivity and radiochemical purity of [^{111}In]US2 in the blood at 1 h postinjection. **(C)** Typical HPLC profile of radioactivity and radiochemical purity of [^{111}In]US2 in the HT-29 tumor at 1 and 24 h postinjection. The HPLC analyses were performed on a Cosmosil C_{18} column (5C_{18}-PAQ, 4.6 × 250 mm) with a solvent of H_2O/MeCN/TFA [90:10:0.1 (0 min) to 60:40:0.1 (30 min)] as the mobile phase at a flow rate of 1 mL/min. Values are expressed as the mean ± standard error of five independent experiments.

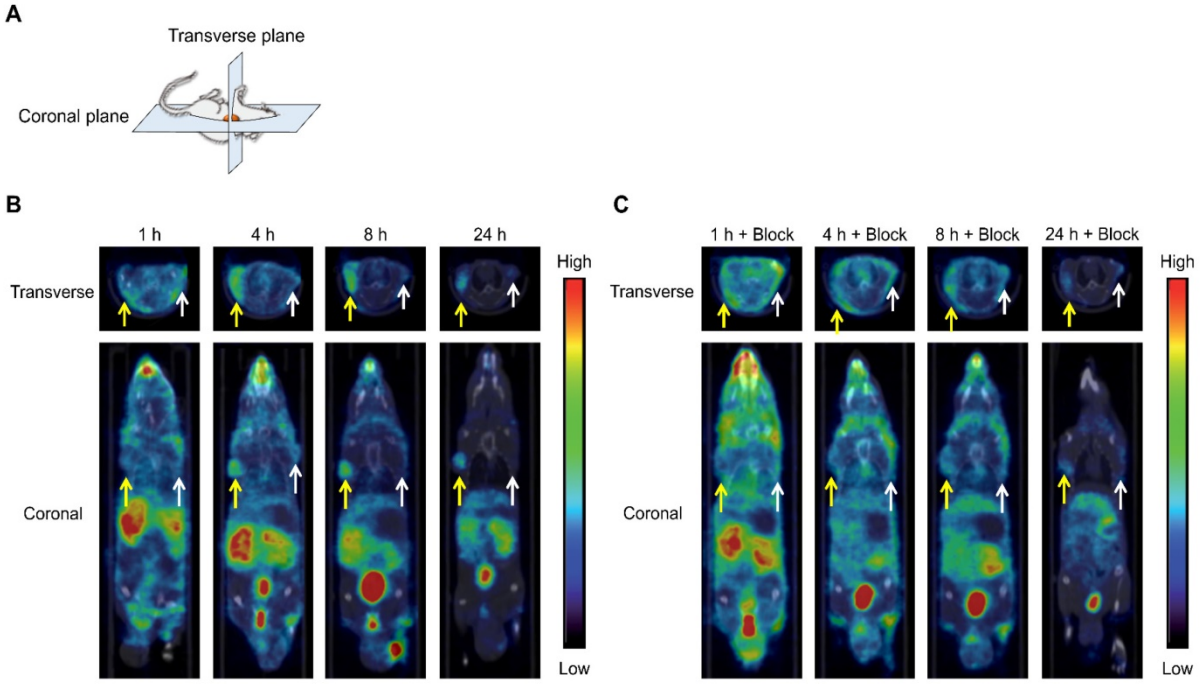

Figure 5. SPECT/CT images of the HT-29 and MDA-MB-231 tumor-bearing mice after [^{111}In]US2 administration. (A) Planes of collected images from mice. **(B)** SPECT/CT images after [^{111}In]US2 administration. **(C)** SPECT/CT images after [^{111}In]US2 administration with acetazolamide (10 mg/kg). Yellow and white arrows indicate the HT-29 and MDA-MB-231 tumors, respectively.

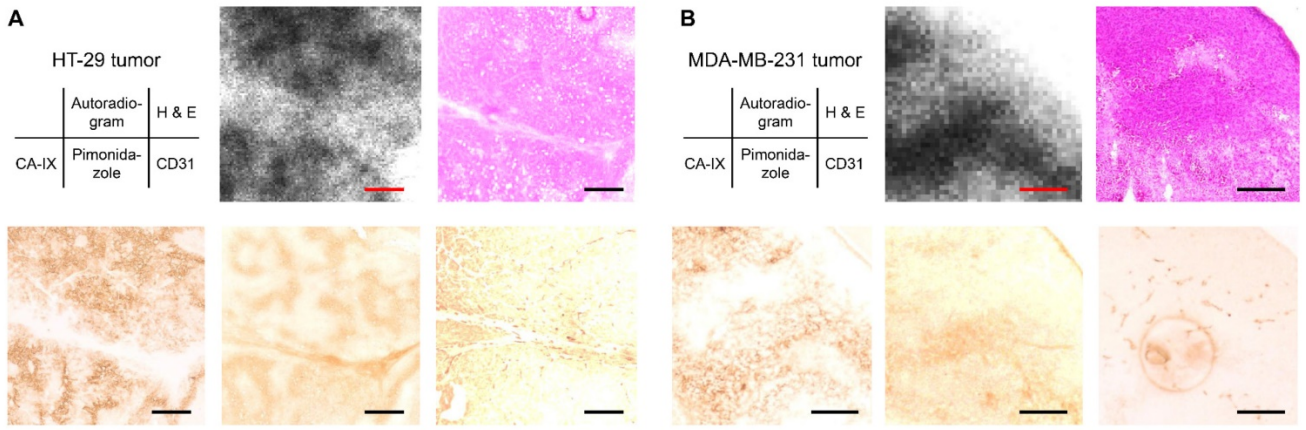

Figure 6. Ex vivo autoradiography with the HT-29 and MDA-MB-231 tumor-bearing mice after [^{111}In]US2 administration. Typical ex vivo autoradiograms of [^{111}In]US2 from the HT-29 **(A)** and MDA-MB-231 **(B)** tumors. The same sections were stained with hematoxylin and eosin (H & E). The adjacent sections were immunostained with anti-CA-IX, pimonidazole, and CD31 antibodies. Scale bars, 500 μm in **(A)** and 250 μm in **(B)**.

Ex vivo autoradiography with model mice

An *ex vivo* autoradiographic examination was performed using the HT-29 and MDA-MB-231 tumor-bearing mice to confirm the binding of [^{111}In]US2 to CA-IX in the tumors (**Figure 6**). The tumors were removed at 4 h postinjection of [^{111}In]US2 for autoradiography. Hypoxic regions within the tumor were confirmed by pimonidazole administration and immunostaining. In the HT-29 tumor, the labeling pattern on autoradiograms of [^{111}In]US2 was consistent with the CA-IX immunohistochemical staining pattern observed in the adjacent tumor sections (**Figure 6A**), indicating the binding of [^{111}In]US2 to CA-IX in the HT-29 tumor. In contrast, radioactivity distribution in the HT-29 tumor was different from the localization of hypoxic regions and blood vessels confirmed by pimonidazole and CD31 immunostaining, respectively. *Ex vivo* autoradiographic experiments using the MDA-MB-231 tumor were also carried out (**Figure 6B**). The accumulation of [^{111}In]US2 in the MDA-MB-231 tumor was consistent with the distribution of CA-IX and hypoxic regions, but not blood vessels, suggesting the detection of CA-IX and hypoxia within the MDA-MB-231 tumor by [^{111}In]US2.

Radionuclide-based therapy

Since we obtained encouraging results using [^{111}In]US2 for CA-IX imaging, radionuclide-based therapy with [^{90}Y]US2 targeting CA-IX was conducted using HT-29 tumor-bearing mice (**Figure 7**). The injected dose of [^{90}Y]US2 ranged from 0 to 7.4 MBq/mouse. The radiotherapeutic effect was evaluated by monitoring the tumor volume in mice three times a week. As shown in **Figure 7C**, the values of the relative tumor volume for mice administered 7.4 and 3.7 MBq of [^{90}Y]US2 were significantly lower compared with those with saline from days 12 and 23 onward, respectively, indicating that radionuclide-based therapy with 7.4 and 3.7 MBq of [^{90}Y]US2 delayed tumor growth. However, no significant difference in the relative tumor volume was observed between mice administered saline and 1.85 MBq of [^{90}Y]US2, suggesting that treatment with 1.85 MBq is not effective for HT-29 tumors. The toxicity of radionuclide-based therapy was evaluated by monitoring the body weight and blood cell counts of mice (**Figure 7D-F**). No marked change in the body weight for mice was observed, indicating the low toxicity of [^{90}Y]US2 (**Figure 7D**). Slight decreases in white blood cell and platelet counts were observed by [^{90}Y]US2 administration, especially in the group receiving high-dose treatment; however, the decreases were not critical, and these counts were recovered within 3 weeks after the injection of the ^{90}Y-complex (**Figure 7E-F**).

Discussion

In mammals, 16 α-CA isozymes or CA-related proteins with a different catalytic activity, subcellular localization, and tissue distribution have been reported. CA-IX is expressed at the extracellular surface, while most CA isozymes are found intracellularly [5, 12, 60, 61], indicating that CA-IX-targeted drug permeability at the cell membrane is a key factor of selectivity for CA-IX over other isozymes. CA-XII is also expressed by the cancer cell surface in response to hypoxia; however, it shows lower expression and catalytic activity as compared with CA-IX [62]. We thus designed and synthesized ^{111}In/^{90}Y complexes comprised of two scaffolds of ureidosulfonamide and DOTA as the CA-IX-binding moiety and ^{111}In/^{90}Y chelator, respectively ([^{111}In/^{90}Y]US2). The bulky structure of the complexes

may contribute to cell impermeability, resulting in their inability to enter the cells and bind to cytosolic CA isozymes, such as highly abundant CA-II, according to Lipinski's rule of five (molecular weight ≥ 500) [63]. To examine the effects of hydrophilicity and CA-IX-ligand valency within complexes on binding and biodistribution, we also prepared and evaluated a monovalent ureidosulfonamide complex, [^{111}In]US1.

The CA-IX expression in HT-29 cells was much higher than that in MDA-MB-231 cells under both normoxic and hypoxic conditions in our study (**Figure 2A**); therefore, HT-29 and MDA-MB-231 cells were used as CA-IX-positive and negative cells, respectively, *in vitro*. However, the high level of CA-IX expression in MDA-MB-231 cells under normoxic conditions has been observed in several studies [64]. The density-dependent CA-IX up-regulation has been demonstrated for several cell lines including MDA-MB-231 [65-67]. Culture conditions with a high cell density might create a pericellular hypoxic environment, leading to the accumulation of HIF-1 and subsequently CA-IX expression. It is difficult to control the pericellular microenvironment completely; therefore, the poor reproducibility of CA-IX expression in MDA-MB-231 cells has been demonstrated [65]. VHL binds to HIF-1α hydroxylated by oxygen, leading to the degradation of HIF-1α and the subsequent prevention of CA-IX expression; therefore, under hypoxic conditions, nonhydroxylated HIF-1α is not recognized by the VHL protein, and RCC4-VHL cells should show CA-IX expression. However, the Western blotting analysis indicated almost no CA-IX expression in RCC4-VHL cells under either normoxic or hypoxic conditions (**Figure S1A**).

Ureidosulfonamide has a much higher affinity for CA than non-substituted sulfonamide [45]; however, few imaging probes based on this scaffold have been reported [44, 68, 69]. The bivalent ureidosulfonamide derivative may show higher affinity compared with any other previously reported probes. As expected, the monovalent ureido-sulfonamide complex with ^{111}In showed a much lower uptake into CA-IX high-expressing cells *in vitro* and tumors *in vivo* than that of [^{111}In]US2 (**Figure 2B-C**, **Figure 3B, D**, and **Figure S1B-C**), suggesting the occurrence of multivalent interactions [57, 58]. Although many nuclear imaging probes including a sulfonamide group targeting CA-IX have been reported over the past few decades, most of them showed limited success regarding their uptake into HT-29 tumors *in vivo* (< 2% injected dose/g) [41, 42, 46, 69-71]. More recently, a higher accumulation of tracers in SK-RC-52 (CA-IX high-expressing) tumors was reported [39, 50]; however, a higher CA-IX expression in the SK-RC-52 cell line than that in HT-29 may largely contribute to the higher uptake of CA-IX ligands in tumors [72]. [^{111}In]US2 showed a higher uptake in the HT-29 tumor than any previously reported CA-IX-targeted imaging probes at 1–4 h postinjection [41, 42, 46, 69-71]. Therefore, we evaluated the utilities of [^{111}In]US2 and [^{90}Y]US2 for CA-IX imaging and cancer radionuclide-based therapy, respectively.

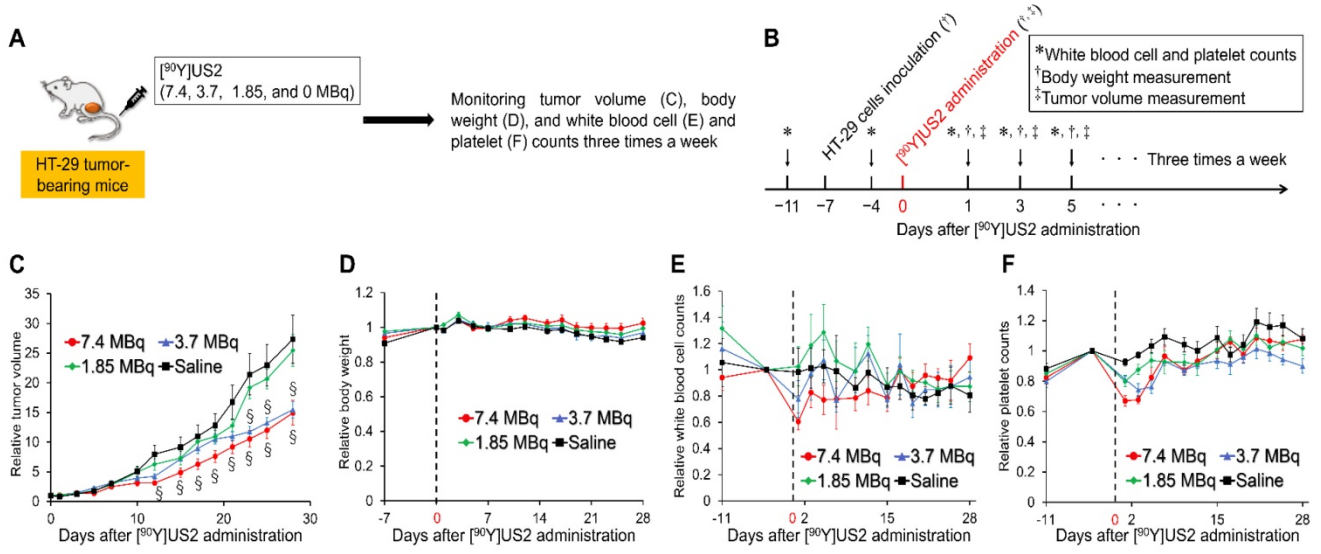

Figure 7. Radionuclide-based therapy of HT-29 tumors in mice administered [^{90}Y]US2. (A) Procedure for a radionuclide-based therapy study. **(B)** Schematic diagram of treatments and measurements in a radionuclide-based therapy study. **(C)** Ratios of the tumor volume for mice to that on the day of [^{90}Y]US2 administration. **(D)** Ratios of the body weight of mice to that on the day of [^{90}Y]US2 administration. **(E)** Ratios of white blood cell counts of mice to that on the day of [^{90}Y]US2 administration. **(F)** Ratios of platelet counts of mice to that on the day of [^{90}Y]US2 administration. Values are expressed as the mean ± standard error of six mice. §$P < 0.05$ compared with untreated mice (Student's *t*-test).

Most of the previously reported theranostic agents for cancer had a nanoparticle platform with very slow pharmacokinetics [16, 17]. Moreover, antibodies comprise a large portion of CA-IX-targeted cancer nuclear imaging or radiotherapeutic agents [35-37, 73]. Their marked retention in normal tissues, such as the blood pool, for several days makes imaging and radionuclide-based therapy difficult due to a low signal-to-background ratio and a radiation burden on normal tissues for a long time, respectively. In contrast, our radiotheranostic agent ([^{111}In/^{90}Y]US2) with its low-molecular-weight showed rapid pharmacokinetics (**Figure 3D, Table S4** and **Table S5**) with high uptake and specificity for CA-IX high-expressing cells *in vitro* and tumors *in vivo* (**Figure 2C** and **Figure 3D**). Although heating was recommended for the radiolabeling of [^{111}In]US2 (**Table S1**), it displayed a very high stability both *in vitro* and *in vivo* (**Figure 4**).

[^{111}In]US2 clearly visualized the HT-29 tumor early in model mice using SPECT, with almost no signal from the CA-IX-negative tumor in the same mice (**Figure 5B**). Moreover, a signal from the HT-29 tumor was blocked with a CA inhibitor, indicating its high *in vivo* specificity for CA (**Figure 5C**). However, *in vivo* blocking studies also indicated the reduction of radioactivity signals in normal tissues. This may be due to the blocking of other CA isozymes, such as CA-IV, which are expressed at the cell surface of various organs and tissues [74], and the diuretic action of acetazolamide. Moreover, the bio-distribution study showed low ratios of radioactivity accumulation within the tumor to those within other normal tissues, such as the kidney and lung, making it difficult to obtain a clear image of such types of cancer. High uptakes into the kidney and lung might be due to the expression of other CA isozymes on the cell surface in these organs [74]. A recent report suggested that the number of binding sites for CA ligands in normal organs might be lower than in the tumor, indicating the possibility of obtaining clearer images by blocking binding sites in normal organs with nonradiolabeled CA ligands at appropriate doses [39]. The accumulation of radioactivity in the HT-29 and MDA-MB-231 tumors was markedly consistent with the localization of CA-IX; however, a poor correlation between the accumulation of [^{111}In]US2 and hypoxic regions in the HT-29 tumor was observed (**Figure 6**). Since the high level of CA-IX expression in the HT-29 cell line was observed even under normoxic conditions (**Figure 2A**), the localization of hypoxia was not consistent with that of CA-IX ([^{111}In]US2) in the HT-29 tumor (**Figure 6A**). Unlike the HT-29 cell line, the MDA-MB-231 cell line showed almost no CA-IX expression under normoxic conditions (**Figure 2A**); therefore, the CA-IX expression in the MDA-MB-231 tumor closely corresponded with hypoxic regions (**Figure 6B**). The weak CA-IX expression in the MDA-MB-231 tumor was consistent with the Western blotting analysis (**Figure 3A**).

Radionuclide-based therapy with [^{90}Y]US2 significantly delayed HT-29 tumor growth without any critical hematological toxicity compared with untreated mice (**Figure 7**). [^{90}Y]US2 administration led to the significant inhibition of HT-29 tumor growth (**Figure 7C**). To our knowledge, this is the first report demonstrating the therapeutic effect of radionuclide-based therapy in HT-29 tumor-bearing mice. Almost no hematological adverse event may occur due to its rapid clearance from the blood pool (**Figure 3D**, **Table S4** and **Table S5**). Nevertheless, as demonstrated in the biodistribution study, moderate radioactivity accumulation within the normal organs, such as the kidney, liver, and stomach, might cause toxicity in such organs. In previous reports of radiotherapeutic effects on cancer models using a ^{90}Y-labeled antibody, such a level of radioactivity accumulation within the normal organs caused no renal or hepatic dysfunction [75, 76]. Therefore, the toxicity of [^{90}Y]US2 in such organs, if any, may be tolerable. Radionuclide-based therapy with [^{90}Y]US2 targets CA-IX (hypoxia) regions of tumors; therefore, combining it with targeted therapy directed at well-oxygenated tumor areas could lead to a more effective cancer therapy, such as that achieving the remission or at least shrinkage of tumors.

Conclusions

In conclusion, we developed novel low-molecular-weight ^{111}In and ^{90}Y complexes based on a bivalent ureidosulfonamide scaffold ([^{111}In/^{90}Y]US2) for cancer radiotheranostics targeting CA-IX overexpressed in hypoxic regions of tumors. [^{111}In]US2 showed specific binding to CA-IX high-expressing cells *in vitro* and tumors *in vivo*, and high *in vitro* and *in vivo* stability. *In vivo*-specific detection of the HT-29 tumor in the mouse was achieved using SPECT with [^{111}In]US2. Moreover, [^{90}Y]US2 administration significantly delayed the tumor growth in cancer models as compared with non-treated mice. Our study has revealed a novel strategy for cancer radiotheranostics with [^{111}In]US2 and [^{90}Y]US2 used for SPECT imaging and radionuclide-based therapy with no critical hematological toxicity, respectively, utilizing CA-IX, leading to more effective, safer, and personalized medicine for cancer patients.

Abbreviations

CA: carbonic anhydrase; CT: computed tomography; DMEM: Dulbecco's modified Eagle's medium; DOTA: 1,4,7,10-tetraazacyclododecane-1,4,7, 10-tetraacetic acid; EDC: 1-ethyl-3-(dimethyl-aminopropyl)carbodiimide; GAPDH: glyceraldehyde 3-phosphate dehydrogenase; H & E: hematoxylin and eosin; HIF-1: hypoxia-inducible factor-1; HOBT: 1-hydroxybenzotriazole; MES: 2-(*N*-morpholino)-ethanesulfonic acid; PBS: phosphate-buffered saline; PBST: phosphate-buffered saline with 0.05% Tween 20; PET: positron emission tomography; RCC4-VA: RCC4 plus vector alone; RCC4-VHL: RCC4 plus von Hippel Lindau; RP-HPLC: reversed-phase high-performance liquid chromatography; SPECT: single photon emission computed tomography; TFA: trifluoroacetic acid; VHL: von Hippel Lindau.

Supplementary Material

Supplementary figures and tables.
http://www.thno.org/v08p2992s1.pdf

Acknowledgement

The study was partially supported by a Grant-in-Aid for Scientific Research (B) (Grant Number 26293274) and a Japan Society for the Promotion of Science (JSPS) Research Fellowship for Young Scientists (16J05493).

Competing Interests

The authors have declared that no competing interest exists.

References

1. Brahimi-Horn MC, Pouyssegur J. Oxygen, a source of life and stress. FEBS Lett. 2007; 581: 3582-91.
2. Hon WC, Wilson MI, Harlos K, Claridge TD, Schofield CJ, Pugh CW, et al. Structural basis for the recognition of hydroxyproline in HIF-1α by pVHL. Nature. 2002; 417: 975-8.
3. Jaakkola P, Mole DR, Tian YM, Wilson MI, Gielbert J, Gaskell SJ, et al. Targeting of HIF-α to the von Hippel-Lindau ubiquitylation complex by O_2-regulated prolyl hydroxylation. Science. 2001; 292: 468-72.
4. Semenza GL. Hypoxia and cancer. Cancer Metastasis Rev. 2007; 26: 223-4.
5. Supuran CT. Carbonic anhydrases: novel therapeutic applications for inhibitors and activators. Nat Rev Drug Discov. 2008; 7: 168-81.
6. Jain RK. Normalization of tumor vasculature: an emerging concept in antiangiogenic therapy. Science. 2005; 307: 58-62.
7. Pries AR, Cornelissen AJ, Sloot AA, Hinkeldey M, Dreher MR, Hopfner M, et al. Structural adaptation and heterogeneity of normal and tumor microvascular networks. PLoS Comput Biol. 2009; 5: e1000394.
8. Wilson WR, Hay MP. Targeting hypoxia in cancer therapy. Nat Rev Cancer. 2011; 11: 393-410.
9. Harris AL. Hypoxia—a key regulatory factor in tumour growth. Nat Rev Cancer. 2002; 2: 38-47.
10. Maxwell PH, Wiesener MS, Chang GW, Clifford SC, Vaux EC, Cockman ME, et al. The tumour suppressor protein VHL targets hypoxia-inducible factors for oxygen-dependent proteolysis. Nature. 1999; 399: 271-5.
11. McDonald PC, Dedhar S. Carbonic anhydrase IX (CAIX) as a mediator of hypoxia-induced stress response in cancer cells. Subcell Biochem. 2014; 75: 255-69.
12. Thiry A, Dogne JM, Masereel B, Supuran CT. Targeting tumor-associated carbonic anhydrase IX in cancer therapy. Trends Pharmacol Sci. 2006; 27: 566-73.
13. Ljungkvist AS, Bussink J, Rijken PF, Raleigh JA, Denekamp J, Van Der Kogel AJ. Changes in tumor hypoxia measured with a double hypoxic marker technique. Int J Radiat Oncol Biol Phys. 2000; 48: 1529-38.
14. Harada H, Inoue M, Itasaka S, Hirota K, Morinibu A, Shinomiya K, et al. Cancer cells that survive radiation therapy acquire HIF-1 activity and translocate towards tumour blood vessels. Nat Commun. 2012; 3: 783.
15. Harada H, Itasaka S, Kizaka-Kondoh S, Shibuya K, Morinibu A, Shinomiya K, et al. The Akt/mTOR pathway assures the synthesis of HIF-1α protein in a glucose- and reoxygenation-dependent manner in irradiated tumors. J Biol Chem. 2009; 284: 5332-42.
16. Kelkar SS, Reineke TM. Theranostics: combining imaging and therapy. Bioconjug Chem. 2011; 22: 1879-903.
17. Satterlee AB, Yuan H, Huang L. A radio-theranostic nanoparticle with high specific drug loading for cancer therapy and imaging. J Control Release. 2015; 217: 170-82.
18. Kratochwil C, Giesel FL, Bruchertseifer F, Mier W, Apostolidis C, Boll R, et al. ^{213}Bi-DOTATOC receptor-targeted alpha-radionuclide therapy induces remission in neuroendocrine tumours refractory to beta radiation: a first-in-human experience. Eur J Nucl Med Mol Imaging. 2014; 41: 2106-19.
19. Scarpa L, Buxbaum S, Kendler D, Fink K, Bektic J, Gruber L, et al. The ^{68}Ga/^{177}Lu theragnostic concept in PSMA targeting of castration-resistant prostate cancer: correlation of SUV_{max} values and absorbed dose estimates. Eur J Nucl Med Mol Imaging. 2017; 44: 788-800.
20. Kratochwil C, Bruchertseifer F, Giesel FL, Weis M, Verburg FA, Mottaghy F, et al. ^{225}Ac-PSMA-617 for PSMA-targeted α-radiation therapy of metastatic castration-resistant prostate cancer. J Nucl Med. 2016; 57: 1941-4.
21. Sansovini M, Severi S, Ambrosetti A, Monti M, Nanni O, Sarnelli A, et al. Treatment with the radiolabelled somatostatin analog ^{177}Lu-DOTATATE for advanced pancreatic neuroendocrine tumors. Neuroendocrinology. 2013; 97: 347-54.
22. Pouyssegur J, Dayan F, Mazure NM. Hypoxia signalling in cancer and approaches to enforce tumour regression. Nature. 2006; 441: 437-43.
23. Ratcliffe PJ, Pugh CW, Maxwell PH. Targeting tumors through the HIF system. Nat Med. 2000; 6: 1315-6.
24. Trastour C, Benizri E, Ettore F, Ramaioli A, Chamorey E, Pouyssegur J, et al. HIF-1α and CA IX staining in invasive breast carcinomas: prognosis and treatment outcome. Int J Cancer. 2007; 120: 1451-8.
25. Parks SK, Chiche J, Pouyssegur J. pH control mechanisms of tumor survival and growth. J Cell Physiol. 2011; 226: 299-308.
26. Swietach P, Hulikova A, Vaughan-Jones RD, Harris AL. New insights into the physiological role of carbonic anhydrase IX in tumour pH regulation. Oncogene. 2010; 29: 6509-21.
27. Stillebroer AB, Mulders PF, Boerman OC, Oyen WJ, Oosterwijk E. Carbonic anhydrase IX in renal cell carcinoma: implications for prognosis, diagnosis, and therapy. Eur Urol. 2010; 58: 75-83.
28. Ord JJ, Agrawal S, Thamboo TP, Roberts I, Campo L, Turley H, et al. An investigation into the prognostic significance of necrosis and hypoxia in high grade and invasive bladder cancer. J Urol. 2007; 178: 677-82.
29. Hutchison GJ, Valentine HR, Loncaster JA, Davidson SE, Hunter RD, Roberts SA, et al. Hypoxia-inducible factor 1α expression as an intrinsic marker of hypoxia: correlation with tumor oxygen, pimonidazole measurements, and outcome in locally advanced carcinoma of the cervix. Clin Cancer Res. 2004; 10: 8405-12.
30. Swietach P, Vaughan-Jones RD, Harris AL. Regulation of tumor pH and the role of carbonic anhydrase 9. Cancer Metastasis Rev. 2007; 26: 299-310.
31. Koukourakis MI, Giatromanolaki A, Sivridis E, Pastorek J, Karapantzos I, Gatter KC, et al. Hypoxia-activated tumor pathways of angiogenesis and pH regulation independent of anemia in head-and-neck cancer. Int J Radiat Oncol Biol Phys. 2004; 59: 67-71.
32. Hussain SA, Ganesan R, Reynolds G, Gross L, Stevens A, Pastorek J, et al. Hypoxia-regulated carbonic anhydrase IX expression is associated with poor survival in patients with invasive breast cancer. Br J Cancer. 2007; 96: 104-9.
33. Swinson DE, Jones JL, Richardson D, Wykoff C, Turley H, Pastorek J, et al. Carbonic anhydrase IX expression, a novel surrogate marker of tumor hypoxia, is associated with a poor prognosis in non-small-cell lung cancer. J Clin Oncol. 2003; 21: 473-82.
34. Dorai T, Sawczuk I, Pastorek J, Wiernik PH, Dutcher JP. Role of carbonic anhydrases in the progression of renal cell carcinoma subtypes: proposal of a unified hypothesis. Cancer Invest. 2006; 24: 754-79.
35. Hoeben BA, Kaanders JH, Franssen GM, Troost EG, Rijken PF, Oosterwijk E, et al. PET of hypoxia with ^{89}Zr-labeled cG250-F(ab')2 in head and neck tumors. J Nucl Med. 2010; 51: 1076-83.
36. Divgi CR, Pandit-Taskar N, Jungbluth AA, Reuter VE, Gonen M, Ruan S, et al. Preoperative characterisation of clear-cell renal carcinoma using iodine-124-labelled antibody chimeric G250 (^{124}I-cG250) and PET in patients with renal masses: a phase I trial. Lancet Oncol. 2007; 8: 304-10.
37. Muselaers CH, Oosterwijk E, Bos DL, Oyen WJ, Mulders PF, Boerman OC. Optimizing lutetium 177-anti-carbonic anhydrase IX radioimmunotherapy in an intraperitoneal clear cell renal cell carcinoma xenograft model. Mol Imaging. 2014; 13: 1-7.
38. Gieling RG, Babur M, Mamnani L, Burrows N, Telfer BA, Carta F, et al. Antimetastatic effect of sulfamate carbonic anhydrase IX inhibitors in breast carcinoma xenografts. J Med Chem. 2012; 55: 5591-600.

39. Krall N, Pretto F, Mattarella M, Muller C, Neri D. A 99mTc-labeled ligand of carbonic anhydrase IX selectively targets renal cell carcinoma in vivo. J Nucl Med. 2016; 57: 943-9.
40. Krall N, Pretto F, Neri D. A bivalent small molecule-drug conjugate directed against carbonic anhydrase IX can elicit complete tumour regression in mice. Chem Sci. 2014; 5: 3640-4.
41. Lau J, Liu Z, Lin KS, Pan J, Zhang Z, Vullo D, et al. Trimeric radiofluorinated sulfonamide derivatives to achieve in vivo selectivity for carbonic anhydrase IX-targeted PET imaging. J Nucl Med. 2015; 56: 1434-40.
42. Lau J, Zhang Z, Jenni S, Kuo HT, Liu Z, Vullo D, et al. PET imaging of carbonic anhydrase IX expression of HT-29 tumor xenograft mice with ^{68}Ga-labeled benzenesulfonamides. Mol Pharm. 2016; 13: 1137-46.
43. Lou Y, McDonald PC, Oloumi A, Chia S, Ostlund C, Ahmadi A, et al. Targeting tumor hypoxia: suppression of breast tumor growth and metastasis by novel carbonic anhydrase IX inhibitors. Cancer Res. 2011; 71: 3364-76.
44. Lv PC, Putt KS, Low PS. Evaluation of nonpeptidic ligand conjugates for SPECT imaging of hypoxic and carbonic anhydrase IX-expressing cancers. Bioconjug Chem. 2016; 27: 1762-9.
45. Pacchiano F, Carta F, McDonald PC, Lou Y, Vullo D, Scozzafava A, et al. Ureido-substituted benzenesulfonamides potently inhibit carbonic anhydrase IX and show antimetastatic activity in a model of breast cancer metastasis. J Med Chem. 2011; 54: 1896-902.
46. Peeters SG, Dubois L, Lieuwes NG, Laan D, Mooijer M, Schuit RC, et al. [^{18}F]VM4-037 microPET imaging and biodistribution of two in vivo CAIX-expressing tumor models. Mol Imaging Biol. 2015; 17: 615-9.
47. Sneddon D, Niemans R, Bauwens M, Yaromina A, van Kuijk SJ, Lieuwes NG, et al. Synthesis and in vivo biological evaluation of ^{68}Ga-labeled carbonic anhydrase IX targeting small molecules for positron emission tomography. J Med Chem. 2016; 59: 6431-43.
48. Minn I, Koo SM, Lee HS, Brummet M, Rowe SP, Gorin MA, et al. [^{64}Cu]XYIMSR-06: A dual-motif CAIX ligand for PET imaging of clear cell renal cell carcinoma. Oncotarget. 2016; 7: 56471-9.
49. Minn I, Lee HS, Koo SM, Ahn HH, Rowe S, Gorin M, et al. [177Lu]XYIMSR-01, a theranostic for targeting carbonic anhydrase IX. J Nucl Med. 2016; 57 (Suppl 2): S53.
50. Yang X, Minn I, Rowe SP, Banerjee SR, Gorin MA, Brummet M, et al. Imaging of carbonic anhydrase IX with an ^{111}In-labeled dual-motif inhibitor. Oncotarget. 2015; 6: 33733-42.
51. Milenic DE, Brady ED, Brechbiel MW. Antibody-targeted radiation cancer therapy. Nature Rev Drug Discov. 2004; 3: 488-99.
52. Srivastava S, Dadachova E. Recent advances in radionuclide therapy. Semin Nucl Med. 2001; 31: 330-41.
53. Schneider CA, Rasband WS, Eliceiri KW. NIH Image to ImageJ: 25 years of image analysis. Nat Methods. 2012; 9: 671-5.
54. De Leon-Rodriguez LM, Kovacs Z, Esqueda-Oliva AC, Miranda-Vera AD. Highly regioselective N-trans symmetrical diprotection of cyclen. Tetrahedron Lett. 2006; 47: 6937-40.
55. Zhang Y, Anderson M, Weisman JL, Lu M, Choy CJ, Boyd VA, et al. Evaluation of diarylureas for activity against plasmodium falciparum. ACS Med Chem Lett. 2010; 1: 460-5.
56. Ivanov S, Liao SY, Ivanova A, Danilkovitch-Miagkova A, Tarasova N, Weirich G, et al. Expression of hypoxia-inducible cell-surface transmembrane carbonic anhydrases in human cancer. Am J Pathol. 2001; 158: 905-19.
57. Iikuni S, Ono M, Watanabe H, Matsumura K, Yoshimura M, Harada N, et al. Enhancement of binding affinity for amyloid aggregates by multivalent interactions of ^{99m}Tc-hydroxamamide complexes. Mol Pharm. 2014; 11: 1132-9.
58. Liu S. Radiolabeled cyclic RGD peptides as integrin $\alpha_v\beta_3$-targeted radiotracers: maximizing binding affinity via bivalency. Bioconjug Chem. 2009; 20: 2199-213.
59. Bao B, Groves K, Zhang J, Handy E, Kennedy P, Cuneo G, et al. In vivo imaging and quantification of carbonic anhydrase IX expression as an endogenous biomarker of tumor hypoxia. PLoS One. 2012; 7: e50860.
60. Smith KS, Ferry JG. Prokaryotic carbonic anhydrases. FEMS Microbiol Rev. 2000; 24: 335-66.
61. Supuran CT, Scozzafava A, Casini A. Carbonic anhydrase inhibitors. Med Res Rev. 2003; 23: 146-89.
62. Neri D, Supuran CT. Interfering with pH regulation in tumours as a therapeutic strategy. Nat Rev Drug Discov. 2011; 10: 767-77.
63. Lipinski CA, Lombardo F, Dominy BW, Feeney PJ. Experimental and computational approaches to estimate solubility and permeability in drug discovery and development settings. Adv Drug Deliv Rev. 2001; 46: 3-26.
64. Jung HS, Han J, Shi H, Koo S, Singh H, Kim HJ, et al. Overcoming the limits of hypoxia in photodynamic therapy: a carbonic anhydrase IX-targeted approach. J Am Chem Soc. 2017; 139: 7595-602.
65. Askoxylakis V, Ehemann V, Rana S, Kramer S, Rahbari NN, Debus J, et al. Binding of the phage display derived peptide CaIX-P1 on human colorectal carcinoma cells correlates with the expression of carbonic anhydrase IX. Int J Mol Sci. 2012; 13: 13030-48.
66. Hunakova L, Bodo J, Chovancova J, Sulikova G, Pastorekova S, Sedlak J. Expression of new prognostic markers, peripheral-type benzodiazepine receptor and carbonic anhydrase IX, in human breast and ovarian carcinoma cell lines. Neoplasma. 2007; 54: 541-8.
67. Sansone P, Piazzi G, Paterini P, Strillacci A, Ceccarelli C, Minni F, et al. Cyclooxygenase-2/carbonic anhydrase-IX up-regulation promotes invasive potential and hypoxia survival in colorectal cancer cells. J Cell Mol Med. 2009; 13: 3876-87.
68. Dubois L, Lieuwes NG, Maresca A, Thiry A, Supuran CT, Scozzafava A, et al. Imaging of CA IX with fluorescent labelled sulfonamides distinguishes hypoxic and (re)-oxygenated cells in a xenograft tumour model. Radiother Oncol. 2009; 92: 423-8.
69. Pan J, Lau J, Mesak F, Hundal N, Pourghiasian M, Liu Z, et al. Synthesis and evaluation of ^{18}F-labeled carbonic anhydrase IX inhibitors for imaging with positron emission tomography. J Enzym Inhib Med Chem. 2014; 29: 249-55.
70. Akurathi V, Dubois L, Celen S, Lieuwes NG, Chitneni SK, Cleynhens BJ, et al. Development and biological evaluation of ^{99m}Tc-sulfonamide derivatives for in vivo visualization of CA IX as surrogate tumor hypoxia markers. Eur J Med Chem. 2014; 71: 374-84.
71. Akurathi V, Dubois L, Lieuwes NG, Chitneni SK, Cleynhens BJ, Vullo D, et al. Synthesis and biological evaluation of a ^{99m}Tc-labelled sulfonamide conjugate for in vivo visualization of carbonic anhydrase IX expression in tumor hypoxia. Nucl Med Biol. 2010; 37: 557-64.
72. Li G, Passebosc-Faure K, Lambert C, Gentil-Perret A, Blanc F, Oosterwijk E, et al. The expression of G250/mn/CA9 antigen by flow cytometry: its possible implication for detection of micrometastatic renal cancer cells. Clin Cancer Res. 2001; 7: 89-92.
73. Muselaers CH, Boers-Sonderen MJ, van Oostenbrugge TJ, Boerman OC, Desar IM, Stillebroer AB, et al. Phase 2 study of lutetium 177-labeled anti-carbonic anhydrase IX monoclonal antibody girentuximab in patients with advanced renal cell carcinoma. Eur Urol. 2016; 69: 767-70.
74. Oosterwijk E. Carbonic anhydrase expression in kidney and renal cancer: implications for diagnosis and treatment. Subcell Biochem. 2014; 75: 181-98.
75. Aung W, Tsuji AB, Sudo H, Sugyo A, Ukai Y, Kouda K, et al. Radioimmunotherapy of pancreatic cancer xenografts in nude mice using ^{90}Y-labeled anti-$\alpha_6\beta_4$ integrin antibody. Oncotarget. 2016; 7: 38835-44.
76. Orozco JJ, Balkin ER, Gooley TA, Kenoyer A, Hamlin DK, Wilbur DS, et al. Anti-CD45 radioimmunotherapy with ^{90}Y but not ^{177}Lu is effective treatment in a syngeneic murine leukemia model. PLoS One. 2014; 9: e113601.